

## Disordered Landau levels of single-cone massless Dirac fermions with broken particle-hole symmetry

Shu-feng Zhang <sup>1,\*</sup>, Yong-liang Song,<sup>1</sup> Wei-jiang Gong,<sup>2</sup> and Chui-zhen Chen <sup>3,†</sup>

<sup>1</sup>*School of Physics and Technology, University of Jinan, Jinan, Shandong 250022, China*

<sup>2</sup>*College of Sciences, Northeastern University, Shenyang 110819, China*

<sup>3</sup>*Institute for Advanced Study and School of Physical Science and Technology, Soochow University, Suzhou 215006, China*



(Received 20 May 2024; revised 6 August 2024; accepted 28 August 2024; published 6 September 2024)

Recently, a single two-dimensional gapless Dirac cone has been experimentally observed on the surface of a semimagnetic topological insulator, providing a platform to study the physics of a single Dirac fermion. Here, we focus on Landau levels (LLs) in the presence of Anderson disorder. We find that the particle-hole (PH) asymmetric term is essential for determining the evolution of LLs with magnetic flux and disorder. With particle-hole symmetry (PHS), the zeroth LL  $E_0$  is pinned at the charge-neutrality point and independent of magnetic field and weak disorder. However, with PHS broken,  $E_0$  either ascends or descends depending on the sign of the PH asymmetric term. Furthermore, neighboring LLs  $E_{n \neq 0}$  adhere to the antilevitation scenario for a vanishing or small PH asymmetric term. In contrast, for a sufficiently large PH asymmetric term, LLs above and below  $E_0$  exhibit different behaviors. We also propose a theoretical method to understand these evolutionary behaviors of disordered LLs based on self-consistent Born approximation. Finally, we find that a rare-region-like effect occurs for a small disorder concentration, leading to rich scenarios. In particular, the zeroth LL  $E_0$  becomes dependent on magnetic flux, and its dependence on disorder strength becomes nonmonotonic. Our findings offer valuable insights for understanding disordered LLs of Dirac fermions and provide guidance for experiments involving topological insulators in strong magnetic fields.

DOI: [10.1103/PhysRevB.110.094202](https://doi.org/10.1103/PhysRevB.110.094202)

### I. INTRODUCTION

Landau levels (LLs) are discrete energy levels that will form in the two-dimensional electron gas (2DEG) subjected to a strong perpendicular magnetic field. These discrete LLs will be broadened by disorder to form separated bands, where all the states are localized except those lying in the center of each LL [1,2]. In fact, it is these extended states that carry nonzero Chern numbers and lead to the integer quantum Hall effect (IQHE). The evolution of these extended states determines the global phase diagram of IQHE [3–6] and is closely related to the localization-delocalization transition [7]. Therefore, it has been an essential issue to answer how these extended states behave at a strong disorder or equivalently a weak magnetic field.

Indeed, the evolution of disordered LLs for the conventional 2DEG has garnered intensive attentions over the decades [8–16]. There exist two well-known scenarios for this evolution: levitation and antilevitation. In a continuous model, the levitation scenario is found to be approximated by  $E_n = \varepsilon_n [1 + 1/(\omega_c \tau)^2]$  [8,9], in which  $E_n$  ( $\varepsilon_n$ ) is the LL in the presence (absence) of disorder,  $\omega_c$  is the magnetic cyclotron frequency, and  $\tau$  is the scattering time due to disorder. This scenario suggests that LLs at the band edge float up to the higher-energy regime with increasing disorder or

decreasing magnetic fields. In contrast, numerical simulations in tight-binding (TB) models offer another possibility: the antilevitation scenario [5,10,15]. In this circumstance, LLs at the band center float towards the edge with increasing disorder until they meet and annihilate with LLs of opposite Chern number at the edge.

With the discovery of graphene [17–19], the study of disordered LLs has sparked renewed interests in Dirac fermions [20–29]. It has been found that LLs  $E_n$  ( $n \neq 0$ ) follow the levitation scenario for the TB model with two Dirac cones [20], while antilevitation scenario exists in the continuous model with a single Dirac cone [21]. Therefore, it seems that the conventional scenarios apply to disordered LLs as well. Nevertheless, the zeroth LL  $E_0$ , which is unique to Dirac fermions, contradicts both levitation and antilevitation scenarios. It is pinned at the Dirac point and remains extended even under strong disorder for the single Dirac cone case [21]. However, in the presence of two Dirac cones, the intervalley scattering causes the two degenerate zeroth LLs to move away from each other [20]. This seems to be consistent with the prediction that the disordered graphene without magnetic field behaves as an insulator in the presence of intervalley scattering [30,31], while it remains metallic if there is only the intravalley scattering [32,33]. Apart from the inconsistent results concerning single and double Dirac cones, particle-hole symmetry (PHS) has been overlooked in previous studies. PHS is not only an important intrinsic symmetry for classifying topological materials [34], but also plays a key role in understanding the band renormalization of topological systems [35,36]. So far,

\*Contact author: sps\_zhangsf@ujn.edu.cn

†Contact author: czchen@suda.edu.cn

the effect of PHS breaking on disordered LLs has not been addressed either in a single or two Dirac cones system.

In this work, we find that breaking PHS significantly alters the evolutionary behaviors of both the zeroth and other LLs in the presence of disorder. We begin with a TB model of the semimagnetic topological insulator (TI) [37–39], featuring a single gapless Dirac cone, and introduce onsite Anderson disorder with concentrations of 100% and 5%. Then, we study how LLs evolve with the PH asymmetric term, strength and concentration of disorder, and magnetic flux. We demonstrate that the zeroth LL  $E_0$ , situated at the Dirac point, remains independent of magnetic flux. It is pinned at the charge-neutrality point even as disorder increases if PHS is preserved. Meanwhile, the neighboring higher LLs adhere to the antilevitation scenario. On the contrary,  $E_0$  moves upward (downward) with increasing disorder for a positive (negative) PH asymmetric term. In this scenario, the neighboring higher LLs may exhibit levitation and antilevitation, depending on the PH asymmetric term. Meanwhile, the neighboring higher LLs adhere to the antilevitation scenario in the presence of weak PH asymmetry. However, LLs at the edges of the conduction and valence bands will follow different scenarios if the PH asymmetric term is sufficiently large. Remarkably, with the introduction of a small concentration of disorder, a rare-region-like effect emerges, causing  $E_0$  to become dependent on magnetic flux and exhibit a nonmonotonic change with disorder strength.

The rest of the paper is organized as follows. Section II describes the model Hamiltonian of the semimagnetic TI and the numerical methods. Section III is the numerical results and discussions. Finally, a brief summary is given in Sec. IV.

## II. MODEL AND METHOD

### A. Model Hamiltonian

The Hamiltonian of a three-dimensional TI discretized in a cubic lattice is written as [40]

$$H = \sum_n \psi_n^\dagger T_0 \psi_n + \sum_{n; j \in \{x, y, z\}} (\psi_n^\dagger T_j \psi_{n+\delta_j} + \text{H.c.}), \quad (1)$$

where  $\psi_n^\dagger = (c_{n1\uparrow}^\dagger, c_{n2\uparrow}^\dagger, c_{n1\downarrow}^\dagger, c_{n2\downarrow}^\dagger)$  with  $c_{n\tau\sigma}^\dagger$  ( $c_{n\tau\sigma}$ ) creating (annihilating) an electron on site  $n$  with orbital  $\tau$  and spin  $\sigma$ .  $(n + \delta_j)$  denotes the site nearest to site  $n$  along  $j$  direction. The Hamiltonian matrix is given as

$$T_0 = (m_0 - 2B_1 - 4B_2)\sigma_0\tau_3 + (C + 6D + \epsilon_n)\sigma_0\tau_0, \quad (2a)$$

$$T_x = -iA_2\sigma_1\tau_1/2 + B_2\sigma_0\tau_3 - D\sigma_0\tau_0, \quad (2b)$$

$$T_y = -iA_2\sigma_2\tau_1/2 + B_2\sigma_0\tau_3 - D\sigma_0\tau_0, \quad (2c)$$

$$T_z = -iA_1\sigma_3\tau_1/2 + B_1\sigma_0\tau_3 - D\sigma_0\tau_0, \quad (2d)$$

in which Pauli matrix  $\sigma$  ( $\tau$ ) acts on spin (orbital) index. The effect of disorder is accounted for by adding a random onsite energy  $\epsilon_n\sigma_0\tau_0$  at each site seating an impurity, where  $\sigma_0$  and  $\tau_0$  are  $2 \times 2$  identity matrices. The onsite energy  $\epsilon_n$  is uniformly distributed in the region  $[-\frac{W}{2}, \frac{W}{2}]$ , with  $W$  representing the strength of disorder. Here,  $cN$  impurities are randomly distributed among  $N$  lattice sites, corresponding to an impurity density of  $c$ . In experiments, the disorder can be realized in realistic materials with a number of randomly

distributed impurities or defects. In this work, the concentration  $c$  describes the ratio of the impurity number to the lattice site number, while  $W$  is used to denote the disorder strength for a given impurity. The randomness of the disorder for the whole sample can be estimated via measuring the electron mobility in the experiment [16]. Moreover, we note that, in the case of dilute impurities, the concentration not only functions as disorder strength but also contributes extra effects, such as rare-region effect [41,42].

To obtain two-dimensional (2D) Dirac cones, the open boundary condition is applied in the  $z$  direction. Then, an onsite Zeeman term  $M_t\sigma_3\tau_0$  is added on each site of the top surface to realize the semimagnetic TI. This can be realized by doping or connecting to a ferromagnetic material in experiments [39]. It gives rise to a gapped topological surface state on the top surface, while a gapless surface state retains on the bottom surface. As a result, we obtain an effective 2D model with only a single gapless Dirac cone.

Additionally, a perpendicular magnetic field is applied along the  $z$  direction to obtain LLs. According to Peierls substitution, the hopping matrix  $T_{i,j}$  between the  $i$ th and  $j$ th sites is replaced by  $T_{i,j}e^{i\frac{e}{\hbar} \int_j^i \vec{A}(\vec{r}) \cdot d\vec{r}}$ , in which  $e$  is the electron charge,  $\hbar$  is the reduced Planck constant, and  $\vec{A}$  is the vector potential. If an electron hops around a minimum square, magnetic field contributes a phase  $\phi = \frac{e}{\hbar} \oint \vec{A}(\vec{r}) \cdot d\vec{r} = \frac{e}{\hbar} \Phi$ , which is proportional to the corresponding magnetic flux  $\Phi$ . For simplicity, we call  $\phi$  as magnetic flux in the following.

In the numerical calculations, we have set  $N_z = 4$ ,  $C = 0$ ,  $m_0 = 1$ ,  $A_1 = A_2 = 1.1$ ,  $A_3 = 1$ ,  $B_1 = B_2 = 0.5$ , and  $M_t = 0.7$ . The PH operation is  $\hat{P} = i\sigma_2\tau_2K$ , in which  $K$  is the operator for complex conjugate. PHS is preserved with  $\hat{P}H(\vec{k})\hat{P}^{-1} = -H(-\vec{k})$  for  $D = 0$ , while broken for a nonzero  $D$ .

### B. Numerical methods

The transfer matrix (TM) method [43] is used to calculate the localization length  $\lambda$ . The system is taken as a long bar with cross section  $N_x \times N_z$  and length  $N_y$ . Periodic and open boundary conditions are adopted in  $x$  and  $z$  directions, respectively. It is in fact a quasi-one-dimensional system and the width  $N_x$  is hereinafter abbreviated as  $N$ . We have set the length  $N_y = 10^4$  and repeated the simulation 100 times with independent disorder configurations. QR factorizations have been performed every 6 TM multiplications. The initial incident wave vector is randomized by performing 200 TM multiplications [44].

The self-consistent Born approximation (SCBA) method [35] is used to determine the Hamiltonian of the effective medium for a disorder strength  $W < 4$ . For Anderson disorder with no spatial correlation, the renormalized self-energy is momentum independent and given by

$$\Sigma(E) = \frac{cW^2}{12} \iint \frac{dk_x dk_y}{(2\pi)^2} \frac{1}{E - H(\vec{k}) - \Sigma(E)}, \quad (3)$$

where  $E$  is the Fermi energy,  $W$  is the strength of disorder and  $c$  the concentration of disorder. All the sites along  $z$  direction are taken as orbital freedom since the open boundary condition is set in this direction.

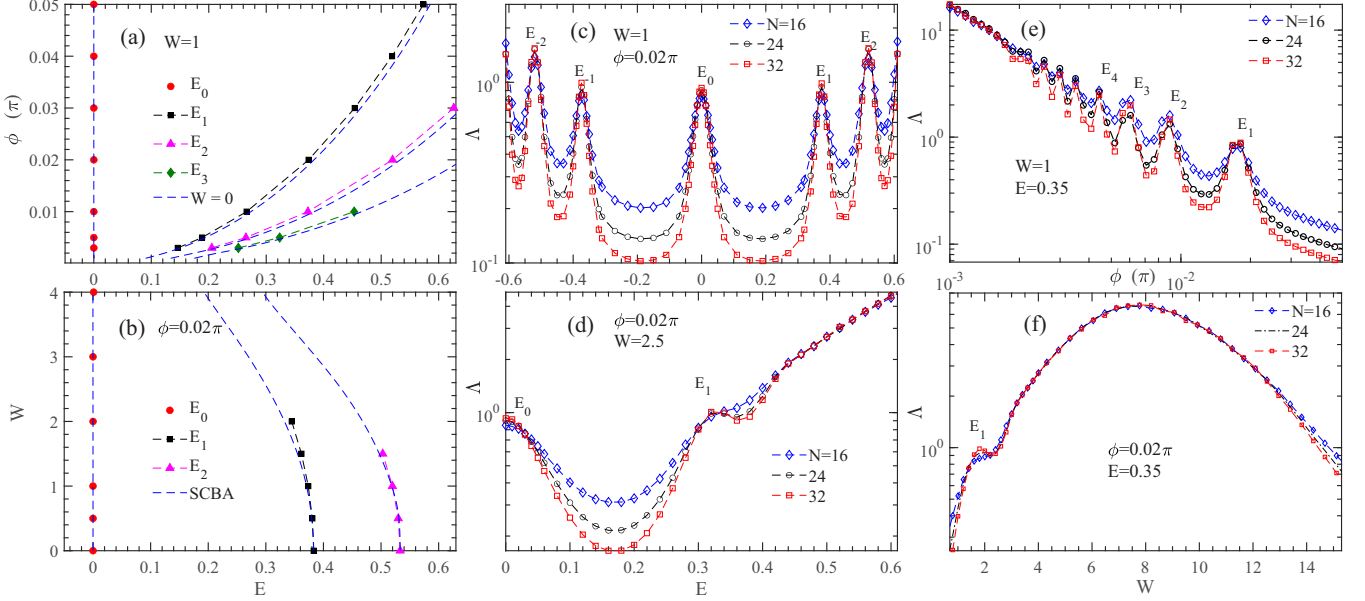


FIG. 1. (a) LL fan diagram with a disorder strength  $W = 1$ . Dashed blue lines correspond to the case with  $W = 0$ . (b) Phase diagram in the  $E$ - $W$  plane with a flux  $\phi = 0.02\pi$ . Dashed blue lines are obtained by SCBA. (c)–(f) The normalized localization length  $\Lambda$  versus Fermi energy  $E$ , flux  $\phi$ , and disorder strength  $W$ , respectively. Parameters:  $D = 0$ ,  $c = 100\%$ . Other parameters given in main text.

LLs can be obtained based on SCBA method as well in the presence of Anderson disorder. In detail, we get an effective Hamiltonian corresponding to each point  $(W, E)$  in the absence of magnetic flux. Then we add a certain flux  $\phi$  and diagonalize the Hamiltonian to obtain the  $n$ th LL  $E_n$  for each point  $(W, E)$ , which is in fact a surface  $E_n = E_n(W, E)$ . Finally, we get the LL  $E_n(W)$  by solving  $E_n(W, E) = E$ .

### III. NUMERICAL RESULTS AND DISCUSSIONS

#### A. PH symmetric case with $c = 100\%$

The numerical results of the normalized localization length  $\Lambda = \lambda/N$ , along with the corresponding evolution of LLs, are depicted in Fig. 1. The system preserves PHS by setting  $D = 0$ , and the Dirac point is located at the energy  $E = 0$ . This symmetry is illustrated in Fig. 1(c), where the curves exhibit symmetry around  $E = 0$  as PHS is also preserved for quantities averaged among different disorder configurations. Therefore, we study only the  $E > 0$  regime in the following if PHS exists.

In general,  $\Lambda = \lambda/N$  increases with size  $N$  in the metallic phase, decreases with  $N$  in the insulating phase, and remains independent of  $N$  at the critical point. In the IQHE, the system forms discrete LLs, and they will be broadened by disorder in a finite-size sample since disorder introduces localized in-gap states near the LLs [1,2]. As a result, there forms a peak feature of  $\Lambda$  and it can be also observed as the peak of the longitudinal conductance or density of states in the experiment [45]. Meanwhile, due to Anderson localization, all states are localized except for a few critical points at the peak centers, which correspond to LL centers. The peak width becomes smaller with increasing the sample size, while the peak center remains unchanged. It indicates that this broadening is a finite-size effect, and the peak will be quite sharp in the thermodynamic limit.

In Fig. 1(c), a series of critical points are observed at the peaks denoted as  $E_0, E_{\pm 1}$ , and  $E_{\pm 2}$ , respectively. Here  $E_0$  is the zeroth LL and  $E_{\pm 1, \pm 2}$  are other neighboring ones. Further, LLs also appear as peaks in Figs. 1(d)–1(f), which show the evolution of  $\Lambda$  against Fermi energy  $E$ , magnetic flux  $\phi$ , and disorder strength  $W$ , respectively. We note that it is difficult to distinguish the peaks of LLs at high-energy regime as shown in Fig. 1(d), weak magnetic field regime in Fig. 1(e), and large  $W$  regime in Fig. 1(f). In these regimes, we have  $\Lambda > 1$  and it seems to be independent of the bar’s width for  $N = 16, 24$ , and 32. The reason may be that the width  $N = 32$  is no longer large enough to distinguish the peak features of  $\Lambda$  for the LLs, where disorder-induced broadening of the LLs exceeds their spacing. Additionally, in Fig. 1(e),  $\log(\Lambda)$  depends linearly on  $\log(\phi)$  once  $\phi$  being small enough, indicative of “divergent” value of  $\Lambda$  for  $\phi = 0$ . It may suggest that the system recovers a Dirac metal behavior with a nonzero disorder  $W = 1$  at a vanishing magnetic flux.

Repeating the calculation of renormalized localization length for several sample sizes at different values of  $\phi$  and  $W$ , we map out the evolution of LLs with magnetic flux  $\phi$  for  $W = 1$  and with disorder strength  $W$  for  $\phi = 0.02\pi$  in Figs. 1(a) and 1(b), respectively. We find that the zeroth LL  $E_0$  remains located at  $E = 0$ , regardless of magnetic flux and disorder strength, at least within the regime  $W \in (0, 4)$ . This is because  $E_0$  is pinned by PHS at the charge-neutrality point. It is consistent with the continuous model of a single-coned Dirac semimetal [21], but different from the two-Dirac-cones case of graphene [20] where intervalley scatterings will split the peak at  $E = 0$ .

Furthermore, we find that LLs  $E_{1,2,3}$  for  $W = 1$  move closer to  $E = 0$  in comparison with the clean case for  $W = 0$ , where LLs are shown as dashed lines in Fig. 1(a) as well. This feature is also found in Fig. 1(b), where LLs  $E_{1,2}$  move downward to  $E = 0$  with disorder increasing in the regime

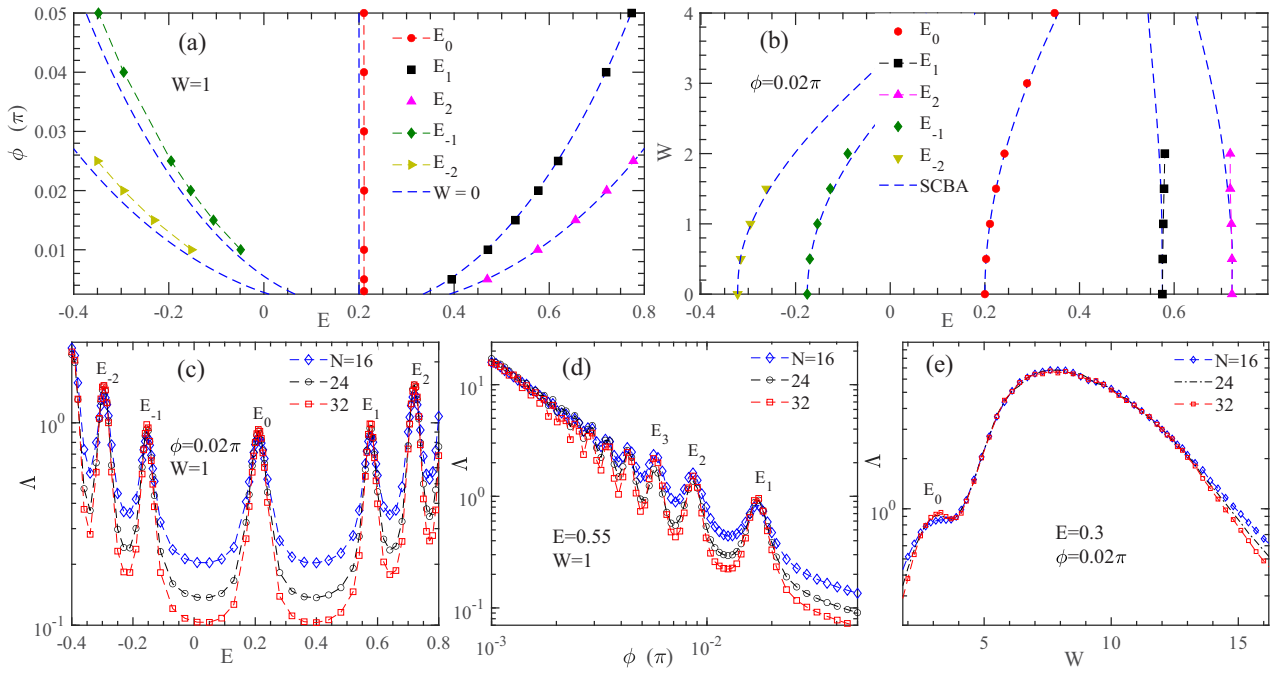


FIG. 2. (a) LL fan diagram with a disorder strength  $W = 1$ . Dashed blue lines correspond to the case with  $W = 0$ . (b) Phase diagram in the  $E$ - $W$  plane with a fixed flux  $\phi = 0.02\pi$ . Dashed blue lines are obtained by SCBA. (c)–(e) The normalized localization length  $\Lambda$  versus  $E$ ,  $\phi$ ,  $W$ , respectively. Parameters:  $D = 0.1$ ,  $c = 100\%$ . Other parameters given in main text.

$W \in (0, 2)$  for  $\phi = 0.02\pi$ . This feature is consistent with the antilevitation scenario, in which LLs at the band edge move away from the band center with increasing disorder due to the mixing between LLs [10]. But it is different from the continuous model of a single-coned Dirac semimetal, where the neighboring LLs  $E_{\pm 1, \pm 2}$  will move away from  $E_0$  [21]. This inconsistency may originate from the difference between the lattice and continuous models since it is similar to the case of 2DEG, where LLs also float up in the continuous model while plunge down in the lattice model with enhancing disorder [8–13]. The evolution of  $E_{0,1,2}$  can be fitted well by numerical results obtained by SCBA, which are displayed as dashed blue lines in Fig. 1(b). Therefore, we conclude that disordered LLs of the gapless Dirac cone with PHS in a lattice model exhibit a unique feature: the zeroth LL remains located at  $E = 0$ , regardless of magnetic flux and disorder strength, while higher LLs manifest an antilevitation scenario.

### B. PH asymmetric case with $c = 100\%$

To investigate the PHS-broken case, we set  $D = 0.1$ , and the Dirac point is shifted to  $E_D = C + \frac{D}{B_1}m_0 = 0.2$  for parameters used in this work [46,47]. The zeroth LL is located at Dirac point  $E_0 = E_D$ , and the other LLs are also shifted by PH asymmetric term  $D$  in the absence of disorder.

In Fig. 2(c), we delve into the study of the normalized localization length as a function of Fermi energy for a disorder strength  $W = 1$  and magnetic flux  $\phi = 0.02\pi$ . The LLs, denoted as  $E_{0, \pm 1, \pm 2}$ , can be distinguished by the peaks in the panel. We observe that the zeroth LL, which is situated at  $E_0 = E_D = 0.2$  in the clean case, undergoes a shift to approximately  $E_0 \approx 0.21$  due to disorder. Furthermore, we

note that the localization length is nearly symmetric about  $E_0$ , albeit not precisely. By repeating this procedure at different values of  $\phi$ , we obtain Fig. 2(a), which displays the LL fan diagram for disorder  $W = 1$ . This diagram closely resembles that of the PHS preserved case in Fig. 1(a), except for the flux-independent zeroth LL, which is shifted to  $E_0 \approx 0.21$ . Moreover, the dependence on flux coincides with the clean case, where LLs are shown as dashed blue lines in Fig. 2(a).

To gain further insights into disordered LLs, the evolution of LLs with varying disorder strength is shown in Fig. 2(b) for  $\phi = 0.02\pi$ . Notably, we find that  $E_0$  floats up with increasing disorder contrasting with the PHS case depicted in Fig. 1(b) and the case of a continuous model [21] where  $E_0$  is pinned at  $E = 0$ . Meanwhile, the neighboring LLs,  $E_{-1, -2}$ , float up with disorder, moving away from the center of the valence band. This aligns with the antilevitation scenario observed in the PHS case. Nevertheless, the two LLs above Dirac points  $E_1$  and  $E_2$  remain nearly independent of  $W$  in the regime  $W \in (0, 2)$ . This unique behavior differs from both the levitation and antilevitation scenarios, contrasting with the case of PHS. Therefore, we conclude that PH asymmetric term is essential to determine disordered LLs. Besides, the peak of  $E_0$  is still clear until  $W = 4$  while those of higher LLs have been smeared for the chosen sample width as shown in Fig. 2(e).  $E_0$  is a well-formed peak at a stronger disorder or smaller sample size, while higher LLs are smeared more easily, as shown in Figs. 1(d), 1(f), and 2(e), respectively.

In order to gain important analytical insights, we perform the SCBA calculation. It is found that the evolution of LLs with disorder is fitted well by LLs obtained by SCBA, which are displayed as dashed blue lines in Fig. 2(b). Especially, the dependence of  $E_0$  on disorder strength  $W^2$  is also shown in

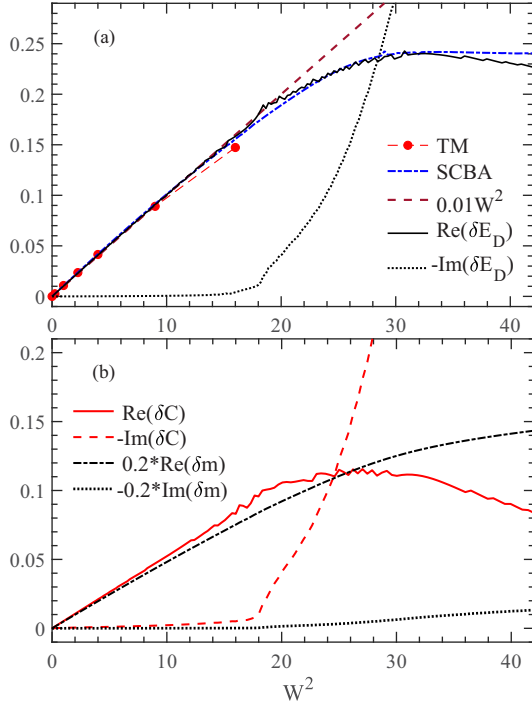


FIG. 3. Numerical results by SCBA. (a) Shows the shift of Dirac point, the zeroth LL obtained by TM method and SCBA, and the linear fitting, respectively. (b) Shows the renormalized parameters in the Hamiltonian corresponding to the zeroth LL. Parameters:  $D = 0.1$ ,  $c = 100\%$ . Other parameters given in main text.

Fig. 3(a). We find that the results from TM method and SCBA can both be fitted to the function

$$\delta E_0 \approx 0.01W^2, \quad (4)$$

where  $\delta E_0 = E_0(W) - E_0(W = 0)$  describes the disorder-induced shift of the zeroth LL  $E_0$ , away from the value of clean case.

To uncover the nature of the shift, we display the corresponding renormalized parameters of the effective Hamiltonian in Fig. 3(b). We find that real components of  $\delta C$  and  $\delta m$  depend linearly on  $W^2$  for  $W < 4$ , while the corresponding imaginary components keep consistently vanishing. Since these parameters change gradually with increasing disorder, it is expected that Dirac point exists and evolves gradually with disorder as well, at least in the weak disorder regime. Since the Dirac point is given by  $E_D \approx C + \frac{D}{B_1}m_0$  for the clean case, the modification is described by  $\delta E_D = \delta C + \frac{D}{B_1}\delta m$ , with numerical results shown in Fig. 3(a). We find that the modification of Dirac point  $\delta E_D$  well follows  $\delta E_0$  determined by TM method for  $W \leq 4$ . The imaginary components of renormalized parameters are also negligible in this regime. These results suggest that the gapless Dirac cone still exists even in the presence of disorder, resulting in a nearly symmetric  $\Lambda$  about  $E_0$  as shown in Fig. 2(c) and a divergent  $\Lambda$  for  $\phi \rightarrow 0$  as shown in Fig. 2(d). Similar with the clean case,  $E_0$  is located at Dirac point and therefore keeps independent of flux at a finite disorder as shown in Fig. 2(a), even though PHS has been broken. This is also consistent with the prediction that a single gapless Dirac cone in graphene remains delocalized

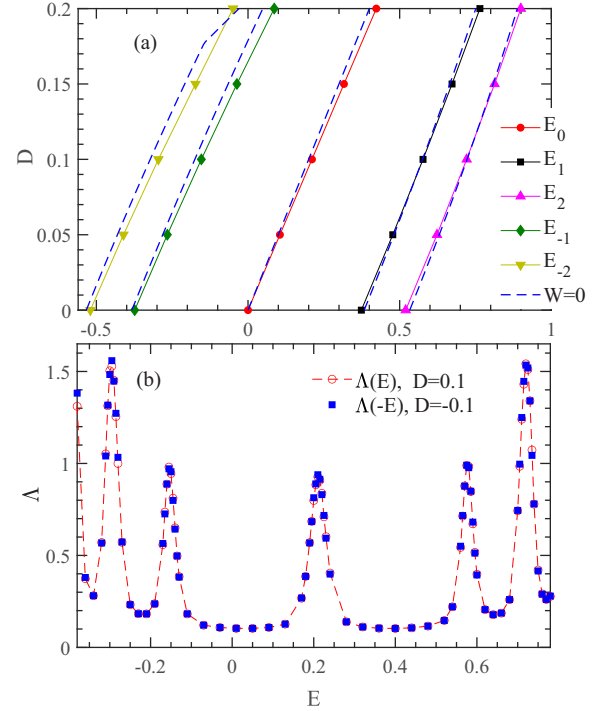


FIG. 4. (a) The evolution of LLs with the PH asymmetric term  $D$ . (b) Renormalized localization length as a function of Fermi energy  $\Lambda(E)$  for  $D = 0.1$ .  $\Lambda(-E)$  is displayed for  $D = -0.1$ . Parameters:  $\phi = 0.02\pi$ ,  $W = 1$ ,  $c = 100\%$ .  $N = 32$  in (b). Other parameters given in main text.

under weak disorder, where the disorder does not mix different valleys [32,33]. Therefore, we conclude that the evolution of LLs for the PH asymmetric case in the presence of weak disorder can also be well understood by the SCBA theory.

Lastly, let us discuss the effect of the PH asymmetric term on the evolution of LLs, as shown in Fig. 4. According to the PH transformation  $\hat{P}H(D)\hat{P}^{-1} = -H(-D)$ , the corresponding eigenvectors are related as  $\psi_{-E, -D} = \hat{P}\psi_{E, D}$ . Therefore, the localization lengths are identical for states at energy  $E$  with parameter  $D$  and those at  $-E$  with the opposite parameter  $-D$ . As shown in Fig. 4(b), we verify that  $\Lambda(E, D) = \Lambda(-E, -D)$  after averaging over 100 disorder configurations. As a result, the behavior of LLs, whether they ascend or descend, depends on the sign of the PH asymmetric term  $D$ . In the light of this relation, we have shown only the evolution of LLs with positive  $D$  in Fig. 4(a). We find that LLs  $E_{0, \pm 1, \pm 2}$  will move upward as  $D$  increases, both in the absence (dashed blue lines) and presence (lines with symbols) of weak disorder. For  $D > 0$ , we consistently find that  $E_0(W = 1)$  always lies to the right of  $E_0(W = 0)$ , indicating that  $E_0$  floats up for  $D > 0$  due to disorder. However, a more comprehensive picture is found for neighboring LLs. For the case of  $D = 0.05$ , a weak disorder will drive  $E_{\pm 1, \pm 2}$  towards  $E_0$ , consistent with the antilevitation scenario observed for  $D = 0$ . On the other hand, for  $D = 0.15$ , both  $E_{-1, -2}$  and  $E_{1, 2}$  will move upward, resulting in antilevitation for  $E_{-1, -2}$  but levitation for  $E_{1, 2}$ . The crossover from antilevitation to levitation for  $E_{1, 2}$  occurs at approximately  $D = 0.1$ . Further, the case of  $D = 0.2$  is similar with that of  $D = 0.15$  except  $E_{-2}$ , which moves

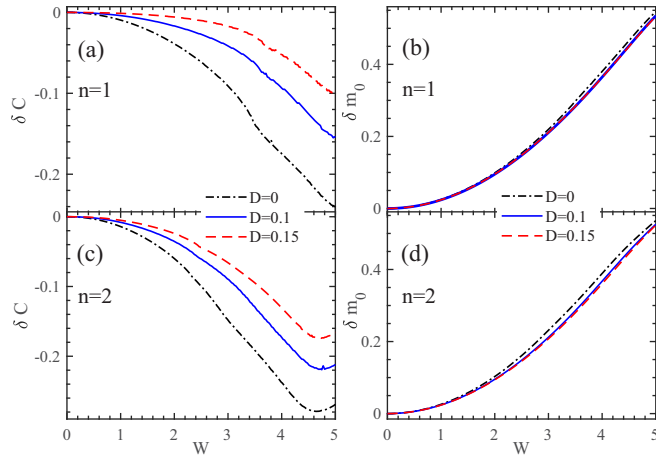


FIG. 5. Renormalized parameters  $\delta C$  (a), (c) and  $\delta m_0$  (b), (d) as a function of disorder strength  $W$ , for the  $n = 1$  (a), (b) and  $n = 2$  (c), (d) LLs, respectively. Parameters:  $c = 100\%$ ,  $\phi = 0$ . Other parameters given in main text.

downward. In fact, further analysis, which is based on the LL fan diagram of a clean system and the spatial distribution of the LL, indicates that  $E_{-2}$  is a LL arising from the bulk states of the sample, rather than from the surface state after the kink shown in the dashed line in Fig. 4(a). The distance between  $E_{-1}$  and  $E_{-2}$  for  $D = 0.2$  is smaller, and the level repulsion becomes dominant to push  $E_{-2}$  downward in the presence of disorder.

The crossover from antilevitation to levitation for  $E_{1,2}$  could be understood by SCBA together with the effective Hamiltonian of the surface state. The effective Hamiltonian is written as [46,47]

$$H_{ss} = C + \frac{Dm_0}{B_1} + D\left(1 - \frac{B_2}{B_1}\right)k^2 + A_2\sqrt{1 - \frac{D^2}{B_1^2}}(\sigma_x k_y - \sigma_y k_x). \quad (5)$$

According to SCBA, which is carried out in a quasi-2D system in the absence of magnetic flux, disorder shifts the surface state only by changing  $C$  and  $m_0$ . Therefore, the shift of the  $n$ th LL  $E_n$  can be approximated as

$$\delta E_n = (\delta C)_n + \frac{D}{B_1}(\delta m_0)_n, \quad (6)$$

in which the index  $n$  on the right side is to note that the renormalized parameter, defined originally on the  $E$ - $W$  plane, is now defined only for the  $n$ th LL, which is the curve  $E = E_n(W)$ . Numerical results, displayed in Fig. 5, show that there is always  $(\delta C)_n < 0$  and  $(\delta m_0)_n > 0$  for  $D = 0, 0.1, 0.15$  and  $n = 1, 2$ , with the imaginary components negligible for a weak disorder. Therefore, the shift depends on the interplay of the first and second terms of Eq. (6). We notice that the first term weakens with  $D$  rising, and the second term is nearly directly proportional to  $D$  since  $\delta m_0$  is not sensitive to  $D$ . Therefore, enhancing  $D$  from zero to a large value will surely change the sign of  $\delta E_{1,2}$  at a certain value of  $D$  and result in the

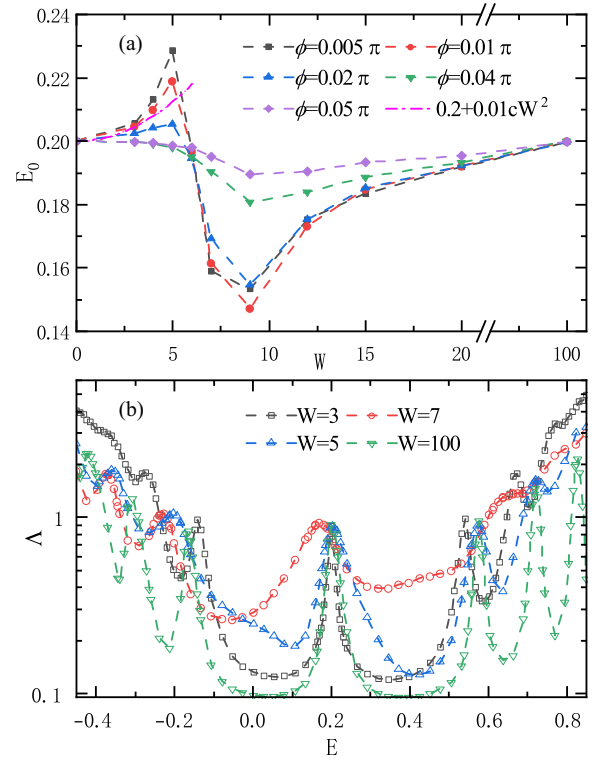


FIG. 6. (a) The zeroth LL  $E_0$  against disorder strength for several magnetic flux. The pink dashed curve is the fitted curve  $E_0 = 0.2 + 0.01 cW^2$  from SCBA. (b) Renormalized localization length for several disorder strengths. Parameters:  $D = 0.1$ ,  $c = 5\%$ ,  $\phi = 0.02\pi$  in (b). Other parameters given in main text.

crossover from antilevitation to levitation, which is  $D \approx 0.1$  for parameters chosen here.

The PH asymmetric term tunes the Dirac point, and it corresponds to the asymmetric band structure, which is commonplace in TIs [39,40]. Generally speaking, the asymmetric band structure can be tuned by band engineering [48,49], such as strain modulation and doping. Especially for the semi-magnetic 3DTI film Cr-doped  $(\text{Bi}_{1-x}, \text{Sb}_x)_2\text{Te}_3$ , it has been verified that the Dirac point for the bottom surface is tunable by changing the Bi:Sb ratio  $x$  [39]. The levitation or antilevitation behaviors could be measured by detecting the evolution of LLs at a vanishing magnetic flux, such as the evolution of longitudinal magnetoresistance minima [16], the Hall plateau transitions [50], and scanning tunneling spectroscopy [28].

### C. PH asymmetric case with diluted disorder

In this section, we aim to investigate the impact of disorder concentration by focusing on the behavior of the zeroth LL,  $E_0$ , at a low disorder concentration. According to the SCBA theory, the evolution of  $E_0$  can be approximated as  $E_0 \approx E_D + 0.01 cW^2$ , obtained by replacing  $W^2$  with  $cW^2$  in Eq. (4). Initially, it may appear that a lower disorder concentration corresponds to a weaker disorder strength. However, further calculations using the TM method reveal a more complex scenario.

Figure 6(a) depicts the evolution of  $E_0$  with disorder strength for various magnetic fluxes. In the weak disorder

regime ( $W \leq 5$ ),  $E_0$  typically increases with disorder strength, although the degree of this increase varies with magnetic flux.  $E_0$  exhibits a more rapid increase compared to the prediction by SCBA (displayed as the pink curve) for small flux values such as  $\phi = 0.005\pi$  and  $0.01\pi$ . Subsequently, the rate of increase diminishes for larger flux values like  $\phi = 0.02\pi$ . Ultimately, for  $\phi = 0.04\pi$  and  $0.05\pi$ ,  $E_0$  tends to stabilize or even experiences a slight decrease within this regime.

In the range  $5 < W < 9$ ,  $E_0$  decreases rapidly and becomes approximately smaller than  $E_D = 0.2$  at  $W = 6$ , irrespective of the magnetic flux. Figure 6(b) shows that for  $W = 5$  and  $7$ ,  $E_{-1}$  moves downward, while  $E_1$  upward, comparing with the  $W = 3$  case. This is different from the result in the case of  $c = 100\%$  shown in Fig. 2(b), where  $E_{-1}$  moves upward while  $E_1$  remains constant. It may suggest that the level-mixing effect between neighboring LLs becomes strong to push the zeroth LL down. By further increasing  $W$  to the regime  $9 < W < 100$ ,  $E_0$  moves upward and converges at 0.2. As depicted in Fig. 6(b), there still exist LLs for disorder as strong as  $W = 100$ . It indicates that a disorder concentration as low as  $c = 5\%$  cannot induce an Anderson phase transition even in a strong disorder limit. When  $W$  is sufficiently large, sites with disorder are broken effectively and can be viewed as hard-wall boundaries. According to the percolation theory [51], the probability of undoped sites being 0.95 is large enough to create a connected region spanning the entire sample. Consequently, electrons are not localized and can transport in the clean region. This also explains why  $E_0$  converges approximately at 0.2. Since this convergence value is less than the maximum located approximately at  $W = 5$ , there will exist a nonmonotonic dependence on  $W$ .

$E_0$  varies with flux for  $c = 5\%$ , while this dependence on flux is absent in the case with  $c = 100\%$ , and this suggests a breakdown of the SCBA theory in the low disorder concentration case. It may be understood by dividing the sample with diluted disorder into two parts, similar with the rare-region effect [41,42]. The sample is considered to be composed of two effective mediums: the doped medium with disorder and the clean medium without disorder. Specifically, the doped medium is a set of several small regions. Each small region contains an impurity at its center and is approximately the size of the magnetic length, which is necessary for the formation of LLs. If two such regions come into contact, they will merge into a larger region. As for the clean medium, it simply consists of all lattice sites that do not belong to the doped medium. With raising flux, magnetic length decreases and LLs will form in a smaller region, which reduces the ratio of the doped medium to the clean one. In the clean medium, we have  $E_0 = E_D = 0.2$ , but  $E_0$  is shifted by disorder in the doped medium. The shift of  $E_0$  of the entire sample, which depends on the ratio of these two mediums, is therefore quantitatively influenced by the magnetic flux, while the qualitative trend, either upward or downward, is unaffected by flux. As a result,  $E_0$  converges closer to  $E_D$  with increasing flux, as the doped medium diminishes and the clean medium becomes dominant.

We have further studied the effect of disorder concentration on this nonmonotonic dependence on  $W$ . Numerical results, displayed in Fig. 7, show that this nonmonotonic behavior occurs for  $c = 10\%$  and  $20\%$  as well. We notice that the

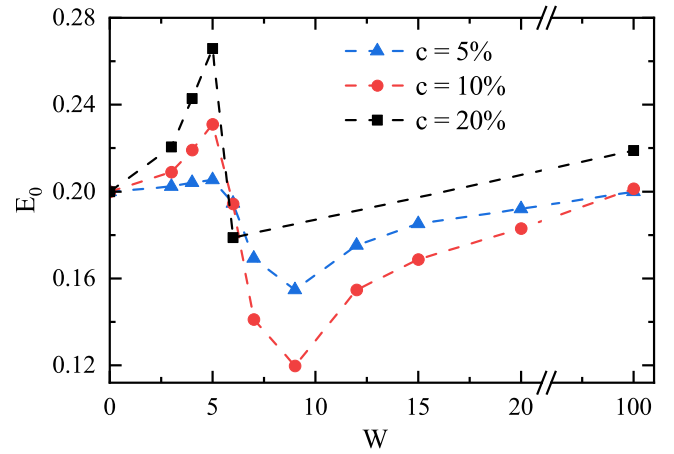


FIG. 7. The zeroth LL  $E_0$  against disorder strength  $W$  for several disorder concentrations  $c$ . Parameters:  $\phi = 0.02\pi$ ,  $D = 0.1$ , others given in main text.

transition occurs in the regime  $5 < W < 6$  for all these three concentrations  $c = 5\%$ ,  $10\%$ , and  $20\%$ , indicating no obvious dependence on disorder concentration. And raising  $c$  enlarges the shift of  $E_0$  but no nonmonotonic dependence on  $c$  is observed at least for  $c < 20\%$ . It further suggests the breakdown of SCBA in the case of diluted disorder since  $c$  is intertwined with  $W$  in the SCBA theory. The effect of disorder concentration could be understood by the proposal of two effective mediums. In the diluted limit, the doped medium consists of small regions separated from each other. Approximately,  $\delta E_0$  is equal in each small region, and it is taken as the shift of the doped medium. The value of  $\delta E_0$  in the diluted limit is estimated from the data for  $c = 5\%$  displayed in Fig. 7. We have  $\delta E_0 > 0$  for  $W < 5$ ,  $\delta E_0 \approx 0$  for  $W = 6$ , and  $\delta E_0 < 0$  for  $7 < W < 20$  in the doped regime, respectively. As the concentration increases, the percentage of doped medium increases as well, quantitatively enhancing the shift of  $E_0$ , and no nonmonotonic dependence on  $c$  is expected. It explains why  $E_0$  arrives at its maximum or minimum at the same disorder strength  $W$ , irrespective of disorder concentration  $c$ . This picture remains valid as long as the assumption of two effective mediums holds, and our numerical findings suggest that it is valid at least for  $c = 20\%$ .

#### IV. CONCLUSION

In summary, we have studied the evolution of LLs with Anderson disorder and magnetic flux in a single-cone gapless Dirac system. We find that  $E_0$  lies at the single-cone Dirac point, which is robust against weak disorder. PH asymmetric term  $D$  is important to determine the evolution of LLs with disorder. With PHS,  $E_0$  is pinned at the charge-neutrality point and independent of weak disorder. With PHS broken,  $E_0$  floats up or shrinks down monotonously for positive or negative  $D$ , respectively. LLs neighboring to  $E_0$  are greatly affected by  $E_0$  to show more complex behaviors inconsistent with conventional 2DEG. In the case with PHS or PH asymmetric term  $D$  is weak, the evolution of  $E_{\pm 1, \pm 2}$  is consistent with antilevitation scenario that LLs at band edge moves away from the band center. With enhancing  $D$ , it changes gradually

into the levitation scenario for  $E_{1,2}$  ( $E_{-1,-2}$ ) while it is still antilevitation for  $E_{-1,-2}$  ( $E_{1,2}$ ) if  $D > 0$  ( $D < 0$ ). Therefore, LLs may follow different scenarios in the gapless Dirac system. As for the dependence on magnetic flux, we find that  $E_0$  is independent of flux while both  $E_{-1,-2}$  and  $E_{1,2}$  move close to  $E_0$  with flux decreasing. This is consistent with the clean case. Besides, we have also studied the effect of the disorder concentration. We find that a rare-region-like effect emerges for diluted disorder. It makes  $E_0$  depend on both magnetic flux and disorder strength.  $E_0$  can not be localized by enhancing disorder strength for the diluted disorder case, and its dependence on disorder strength becomes nonmonotonic, which may be understood by our proposal of dividing the system into two effective mediums.

## ACKNOWLEDGMENTS

This work was supported by the National Natural Science Foundation of China (Grants No. 12104183, No. 52173283), the National Key R&D Program of China (Grant No. 2022YFA1403700), Shandong Provincial Natural Science Foundation (Grant No. ZR2021MA040), Taishan Scholar Program of Shandong Province (Grant No. ts20190939), the Natural Science Foundation of Jiangsu Province (Grant No. BK20230066), Jiangsu Shuang Chuang Project (JSS-CTD202209) and the Priority Academic Program Development (PAPD) of Jiangsu Higher Education Institution. The numerical calculations were supported by the high performance computing platform at university of Jinan.

- [1] B. Huckestein, Scaling theory of the integer quantum Hall effect, *Rev. Mod. Phys.* **67**, 357 (1995).
- [2] *The Quantum Hall Effect*, edited by R. E. Prange and S. M. Girvin (Springer, New York, 1990).
- [3] S. Kivelson, D. H. Lee, and S. C. Zhang, Global phase diagram in the quantum Hall effect, *Phys. Rev. B* **46**, 2223 (1992).
- [4] G. Xiong, S. D. Wang, Q. Niu, D. C. Tian, and X. R. Wang, Metallic phase in quantum Hall systems due to inter-Landau-band mixing, *Phys. Rev. Lett.* **87**, 216802 (2001).
- [5] D. Z. Liu, X. C. Xie, and Q. Niu, Weak field phase diagram for an integer quantum Hall liquid, *Phys. Rev. Lett.* **76**, 975 (1996).
- [6] H. L. Li, C. Z. Chen, H. Jiang, and X. C. Xie, Coexistence of quantum Hall and quantum anomalous Hall phases in disordered  $\text{MnBi}_2\text{Te}_4$ , *Phys. Rev. Lett.* **127**, 236402 (2021).
- [7] F. Evers and A. D. Mirlin, Anderson transitions, *Rev. Mod. Phys.* **80**, 1355 (2008).
- [8] R. B. Laughlin, Levitation of extended-state bands in a strong magnetic field, *Phys. Rev. Lett.* **52**, 2304 (1984).
- [9] D. E. Khmelnitakii, Quantum Hall effect and additional oscillations of conductivity in weak magnetic fields, *Phys. Lett. A* **106**, 182 (1984).
- [10] X. C. Xie, D. Z. Liu, B. Sundaram, and Q. Niu, Transition from the integer quantum Hall state to the insulator state, *Phys. Rev. B* **54**, 4966 (1996).
- [11] K. Yang and R. N. Bhatt, Floating of extended states and localization transition in a weak magnetic field, *Phys. Rev. Lett.* **76**, 1316 (1996).
- [12] D. N. Sheng, Z. Y. Weng, and X. G. Wen, Float-up picture of extended levels in the integer quantum Hall effect: A numerical study, *Phys. Rev. B* **64**, 165317 (2001).
- [13] Th. Koschny, H. Potempa, and L. Schweitzer, Levitation of current carrying states in the lattice model for the integer quantum Hall effect, *Phys. Rev. Lett.* **86**, 3863 (2001).
- [14] M. Ortuno, A. M. Somoza, V. V. Mkhitarian, and M. E. Raikh, Phase diagram of the weak-magnetic-field quantum Hall transition quantified from classical percolation, *Phys. Rev. B* **84**, 165314 (2011).
- [15] C. Wang, Y. Avishai, Y. Meir, and X. R. Wang, Anti-levitation in integer quantum Hall systems, *Phys. Rev. B* **89**, 045314 (2014).
- [16] W. Pan, K. W. Baldwin, K. W. West, L. N. Pfeiffer, and D. C. Tsui, Antilevitation of Landau levels in vanishing magnetic fields, *Phys. Rev. B* **94**, 161303(R) (2016).
- [17] K. S. Novoselov, A. K. Geim, S. V. Morozov, D. Jiang, M. I. Katsnelson, I. V. Grigorieva, S. V. Dubonos, and A. A. Firsov, Two-dimensional gas of massless Dirac fermions in graphene, *Nature (London)* **438**, 197 (2005).
- [18] Y. Zhang, Y. W. Tan, H. L. Stormer, and P. Kim, Experimental observation of the quantum Hall effect and Berry's phase in graphene, *Nature (London)* **438**, 201 (2005).
- [19] A. H. C. Neto, F. Guinea, N. M. R. Peres, K. S. Novoselov, and A. K. Geim, The electronic properties of graphene, *Rev. Mod. Phys.* **81**, 109 (2009).
- [20] D. N. Sheng, L. Sheng, and Z. Y. Weng, Quantum Hall effect in graphene: Disorder effect and phase diagram, *Phys. Rev. B* **73**, 233406 (2006).
- [21] K. Nomura, S. Ryu, M. Koshino, C. Mudry, and A. Furusaki, Quantum Hall effect of massless Dirac fermions in a vanishing magnetic field, *Phys. Rev. Lett.* **100**, 246806 (2008).
- [22] E. J. König, P. M. Ostrovsky, I. V. Protodopov, I. V. Gornyi, I. S. Burmistrov, and A. D. Mirlin, Half-integer quantum Hall effect of disordered Dirac fermions at a topological insulator surface, *Phys. Rev. B* **90**, 165435 (2014).
- [23] D. L. Miller, K. D. Kubista, G. M. Rutter, M. Ruan, W. A. de Heer, P. N. First, and J. A. Stroscio, Observing the quantization of zero mass carriers in graphene, *Science* **324**, 924 (2009).
- [24] T. Hanaguri, K. Igarashi, M. Kawamura, H. Takagi, and T. Sasagawa, Momentum-resolved Landau-level spectroscopy of Dirac surface state in  $\text{Bi}_2\text{Se}_3$ , *Phys. Rev. B* **82**, 081305(R) (2010).
- [25] Y. Okada, M. Serbyn, H. Lin, D. Walkup, W. Zhou, C. Dhital, M. Neupane, S. Xu, Y. J. Wang, R. Sankar, F. Chou, A. Bansil, M. Z. Hasan, S. D. Wilson, L. Fu, and V. Madhavan, Observation of Dirac node formation and mass acquisition in a topological crystalline insulator, *Science* **341**, 1496 (2013).
- [26] B. E. Feldman, M. T. Randeria, A. Gyenis, F. Wu, H. Ji, R. J. Cava, A. H. MacDonald, and A. Yazdani, Observation of a nematic quantum Hall liquid on the surface of bismuth, *Science* **354**, 316 (2016).
- [27] A. Uri, S. Grover, Y. Cao, J. A. Crosse, K. Bagani, D. Rodan-Legrain, Y. Myasoedov, K. Watanabe, T. Taniguchi, P. Moon, M. Koshino, P. Jarillo-Herrero, and E. Zeldov, Mapping the twist-angle disorder and Landau levels in magic-angle graphene, *Nature (London)* **581**, 47 (2020).

- [28] J. X. Yin, W. Ma, T. A. Cochran, X. Xu, S. S. Zhang, H. J. Tien, N. Shumiya, G. Cheng, K. Jiang, B. Lian, Z. Song, G. Chang, I. Belopolski, D. Multer, M. Litskevich, Z. J. Cheng, X. P. Yang, B. Swidler, H. Zhou, H. Lin *et al.*, Quantum-limit Chern topological magnetism in  $\text{TbMn}_6\text{Sn}_6$ , *Nature (London)* **583**, 533 (2020).
- [29] D. A. Kozlov, J. Ziegler, N. N. Mikhailov, Z. D. Kvon, and D. Weiss, Spin splitting and disorder of Landau levels in HgTe-based Dirac fermions, *Phys. Rev. B* **108**, L241301 (2023).
- [30] I. L. Aleiner and K. B. Efetov, Effect of disorder on transport in graphene, *Phys. Rev. Lett.* **97**, 236801 (2006).
- [31] A. Altland, Low-energy theory of disordered graphene, *Phys. Rev. Lett.* **97**, 236802 (2006).
- [32] K. Nomura, M. Koshino, and S. Ryu, Topological delocalization of two-dimensional massless Dirac fermions, *Phys. Rev. Lett.* **99**, 146806 (2007).
- [33] J. H. Bardarson, J. Tworzydło, P. W. Brouwer, and C. W. J. Beenakker, One-parameter scaling at the Dirac point in graphene, *Phys. Rev. Lett.* **99**, 106801 (2007).
- [34] C. K. Chiu, J. C. Y. Teo, A. P. Schnyder, and S. Ryu, Classification of topological quantum matter with symmetries, *Rev. Mod. Phys.* **88**, 035005 (2016).
- [35] C. W. Groth, M. Wimmer, A. R. Akhmerov, J. Tworzydło, and C. W. J. Beenakker, Theory of the topological Anderson insulator, *Phys. Rev. Lett.* **103**, 196805 (2009).
- [36] H. M. Guo, G. Rosenberg, G. Refael, and M. Franz, Topological Anderson insulator in three dimensions, *Phys. Rev. Lett.* **105**, 216601 (2010).
- [37] R. Yoshimi, K. Yasuda, A. Tsukazaki, K. S. Takahashi, N. Nagaosa, M. Kawasaki, and Y. Tokura, Quantum Hall states stabilized in semi-magnetic bilayers of topological insulators, *Nat. Commun.* **6**, 8530 (2015).
- [38] R. Lu, H. Sun, S. Kumar, Y. Wang, M. Gu, M. Zeng, Y.-J. Hao, J. Li, J. Shao, X.-M. Ma, Z. Hao, K. Zhang, W. Mansuer, J. Mei, Y. Zhao, C. Liu, K. Deng, W. Huang, B. Shen, K. Shimada, E. F. Schwier, C. Liu, Q. Liu, and C. Chen, Half-magnetic topological insulator with magnetization-induced Dirac gap at a selected surface, *Phys. Rev. X* **11**, 011039 (2021).
- [39] M. Mogi, Y. Okamura, M. Kawamura, R. Yoshimi, K. Yasuda, A. Tsukazaki, K. S. Takahashi, T. Morimoto, N. Nagaosa, M. Kawasaki, Y. Takahashi, and Y. Tokura, Experimental signature of parity anomaly in semi-magnetic topological insulator, *Nat. Phys.* **18**, 390 (2022).
- [40] H. J. Zhang, C. X. Liu, X. L. Qi, X. Dai, Z. Fang, and S. C. Zhang, Topological insulators in  $\text{Bi}_2\text{Se}_3$ ,  $\text{Bi}_2\text{Te}_3$ , and  $\text{Sb}_2\text{Te}_3$  with a single Dirac cone on the surface, *Nat. Phys.* **5**, 438 (2009).
- [41] T. Vojta, Rare region effects at classical, quantum, and non-equilibrium phase transitions, *J. Phys. A: Math. Gen.* **39**, R143 (2006).
- [42] H. Ji, H. Liu, H. Jiang, and X. C. Xie, Disorder effects on quantum transport and quantum phase transition in low-dimensional superconducting and topological systems, *Adv. Phys. X* **6**, 1884133 (2021).
- [43] A. MacKinnon and B. Kramer, The scaling theory of electrons in disordered solids: Additional numerical results, *Z. Phys. B* **53**, 1 (1983).
- [44] K. Slevin, Y. Asada, and L. I. Deych, Fluctuations of the Lyapunov exponent in two-dimensional disordered systems, *Phys. Rev. B* **70**, 054201 (2004).
- [45] *50 Years of Anderson Localization*, edited by E. Abrahams (World Scientific, Singapore, 2010).
- [46] W. Y. Shan, H. Z. Lu, and S. Q. Shen, Effective continuous model for surface states and thin films of three-dimensional topological insulators, *New J. Phys.* **12**, 043048 (2010).
- [47] H. Z. Lu, W. Y. Shan, W. Yao, Q. Niu, and S. Q. Shen, Massive Dirac fermions and spin physics in an ultrathin film of topological insulator, *Phys. Rev. B* **81**, 115407 (2010).
- [48] J. Zhang, C.-Z. Chang, Z. Zhang, J. Wen, X. Feng, K. Li, M. Liu, K. He, L. Wang, X. Chen, Q.-K. Xue, X. Ma, and Y. Wang, Band structure engineering in  $(\text{Bi}_{1-x}\text{Sb}_x)_2\text{Te}_3$  ternary topological insulators, *Nat. Commun.* **2**, 574 (2011).
- [49] G. G. Naumis, S. Barraza-Lopez, M. Oliva-Leyva, and H. Terrones, Electronic and optical properties of strained graphene and other strained 2D materials: a review, *Rep. Prog. Phys.* **80**, 096501 (2017).
- [50] I. Glazman, C. E. Johnson, and H. W. Jiang, Fate of the delocalized states in a vanishing magnetic field, *Phys. Rev. Lett.* **74**, 594 (1995).
- [51] M. Li, R.-R. Liu, L. Lv, M.-B. Hu, S. Xu, and Y.-C. Zhang, Percolation on complex networks: Theory and application, *Phys. Rep.* **907**, 1 (2021).